Ferroptosis-Related Long Non-Coding RNAs and the Roles of LASTR in Stomach Adenocarcinoma

Gongjun Wang
Qingdao University Medical College
Libin Sun
The Affiliated Hospital of Qingdao University
Shasha Wang
The Affiliated Hospital of Qingdao University
Jing Guo
The Affiliated Hospital of Qingdao University
Hui Li
Qingdao University Medical College
Ruoxi Xiao
Qingdao University Medical College
Wenqian Li
Qingdao University Medical College
Jing Lv
The Affiliated Hospital of Qingdao University
Wensheng Qiu
The Affiliated Hospital of Qingdao University https://orcid.org/0000-0002-5063-7830
Weiwei Qi (qwwdz@126.com)
The Affiliated Hospital of Qingdao University https://orcid.org/0000-0002-3262-1560

Primary research

Keywords: stomach adenocarcinoma, TCGA, ferroptosis, lncRNA, prognosis signature, LASTR

Posted Date: October 5th, 2021

DOI: https://doi.org/10.21203/rs.3.rs-714235/v1

Version of Record: A version of this preprint was published at Molecular Medicine Reports on February 8th, 2022. See the published version at https://doi.org/10.3892/mmr.2022.12634.

Abstract

Background: Ferroptosis is a form of cell death involved in diverse physiological context. Increasing evidence suggests that there is a closely regulatory relationship between ferroptosis and long noncoding RNAs (lncRNAs).

Method: RNA-sequencing data from The Cancer Genome Atlas (TCGA) data resource and ferroptosis-related genes from FerrDb (http://www.zhounan.org/ferrdb/) data resource were employed to select differentially expressed lncRNAs. We performed Univariate Cox regression and multivariate Cox analyses analysis on these differentially expressed lncRNAs to screen independent predictive factors. Subsequently, we established two signatures for predicting overall survival (OS) and progression-free survival (PFS). Finally, experiments were conducted to verify the roles of LASTR in gastric cancer (GC).

Results: We identified 12 differentially expressed lncRNAs linked with OS and 13 associated with PFS. Kaplan-Meier(K-M) analyses exhibited that the high-risk group was related to a poor prognosis of stomach adenocarcinoma (STAD). The AUCs of the OS, as well as PFS signatures of lncRNAs were 0.734 and 0.771, respectively, indicating their excellent efficacy in predicting STAD prognosis. Our experimental results illustrated that the inhibition of LASTR inhibited tumor proliferation and migration in GC.

Conclusion: This comprehensive evaluation of the ferroptosis-related lncRNA landscape in STAD unearthed novel lncRNAs related to carcinogenesis. In addition, we also experimentally confirmed the effects of LASTR on proliferation, migration and ferroptosis. These results provide potential novel targets for tumor treatment and promote personalized medicine.

Introduction

Gastric cancer (GC) treatment remains an important challenge as this disease threatens human health worldwide. GC has the 5th highest cancer incidence and the third highest cancer mortality rates in the world (1). GC is the second most prevalent cancer in China. In 2015, there were about 679,100 new cases along with 498,000 deaths, causing a considerable burden to society (2). Because most individuals are already in the advanced stage when they are diagnosed and based on the incidences of chemotherapy resistance and recurrence, the overall five-year OS of patients is less than 25% (3). Therefore, identification of its underlying pathogenic mechanism and the detection of novel and reliable potential therapeutic targets are essential to enhance prognosis of individuals with GC.

The roles of ferroptosis in tumors have attracted increasing attention recently. Ferroptosis is an iron-dependent mechanism of cell death that has been recently discovered (4). The primary mechanism of ferroptosis depends on the action of ester oxygenase or divalent iron, which catalyze lipid peroxidation of unsaturated fatty acids, hence triggering cell death. Besides, it also functions in the antioxidant system (the glutathione system) to regulate the reduction of the core enzyme–phospholipid hydroperoxide glutathione peroxidase 4 (GPX4)(5, 6). Increasing studies have shown that lncRNAs can regulate ferroptosis and mediate the biological behavior in various tumors. Zhang et al. documented that lncRNA

OIP5-AS1 induced ferroptosis resistance and promoted prostate cancer progression (7). Ma et al. proved that the long noncoding RNA MEG8 repressed proliferation, as well as induces ferroptosis in hemangioma endothelial cells (8). The long noncoding RNA LINC00618 was reported to accelerate ferroptosis via increasing the contents of lipid reactive oxygen species and iron in human leukemia (9). However, there is still a lack of research that systematically assesses ferroptosis-related lncRNA signatures and explains their relationship with OS and PFS in STAD patients.

Herein, we established two signatures consisting of differentially expressed ferroptosis-related lncRNAs to evaluate OS and PFS prognosis based on TCGA data. Furthermore, experiments were conducted to validate the functions of a unique overlapping lncRNA (LASTR) of the signatures for PFS and OS in GC.

Methods

Data collection

RNA-sequence data of 407 patients (32 non-malignant and 375 tumor) were abstracted from the TCGA-STAD data resource. TCGA constitutes a publicly funded project whose purpose includes cataloging and discovering major cancer-pathogenesis genome changes in large data sets of over 30 human cancer types via large-scale genome sequencing along with integrated multidimensional analyses. Herein, the matching TCGA clinical data were abstracted from the cBioPortal (http://www.cbioportal.org/) (10). The matching ferroptosis-related lncRNAs were abstracted from FerrDb (11), an online consortium providing a comprehensive, as well as up-to-date data resource for ferroptosis biomarkers, their modulatory molecules along with the linked diseases.

Profiling differentially expressed ferroptosis-related lncRNAs (DEFRLs)

To determine ferroptosis-related lncRNAs, we employed to limma R tool to conduct differential analyses for the STAD samples from TCGA. The remarkable differences in expressions were determined using the FDR < 0.05 and |log2FC|≥1 threshold. Pearson correlation was adopted to determine the relationship of the lncRNAs with ferroptosis markers. A correlation coefficient of $|R^2|>0.45$ at $P < 0.05$ signified remarkable relationship.

Functional enrichment analysis of DEFRLs

The clusterprofle R tool was employed to perform Gene Ontology (GO) coupled with Kyoto Encyclopedia of Genes and Genomes (KEGG) to elucidate the role of unrecovered DEFRLs (12). An adjusted $P < 0.05$ denoted statistical significance.

Development of the ferroptosis-related lncRNA prognostic signatures

We analyzed OS along with PFS to gain insights into the prognostic significance of DEFRLs in individuals with STAD. We defined OS as the time beginning from the first day of diagnosis to death from any cause, whilst PFS included the time from the day of diagnosis to the time of cancer progression or death. Firstly,

a univariate Cox analysis was adopted to explore OS- along with PFS-related DEFRLs. Secondly, multivariate Cox regression was employed to determine the potential OS- along with PFS-related DEFRLs to create two predictive signatures, referred to as the OS signature and the PFS signature, respectively. The DEFRLs' coefficients in the final signatures were validated simultaneously and utilized to compute the risk scores for each STAD patient. And all subjects were stratified into either low-risk group or high-risk group, as per the median score. The risk score was calculated as follows:

$$\text{Risk Score} = \sum_{i=0}^{n} \beta i * Gi$$

βi is the coefficient of lncRNA i in the multivariate Cox analysis; Gi is the expression value of lncRNA i; and n is the number of lncRNAs in the signature.

To explore the efficiency of the signatures, the "survival ROC" tool was employed to create ROC (receiver operating characteristic) curves at one-, three-, and five-years, and the matching time-based AUCs (area under the curves) were computed. And we generated the K-M survival plots with the log-rank test to assess the differences in OS and PFS between high- and low-risk group.

The predictive nomogram integrating DEFRL signatures and clinical variables

Clinical characteristics, including gender, age, grade and stage were abstracted from the cBioPortal data resource. Univariate Cox regression integrating the signature with the clinical information was conducted for individuals with STAD, and factors harboring $P < 0.05$ were subjected to multivariate regression to determine the independent predictive factors. After that, two predictive nomograms were created using the R "rms" package on the basis of the independent predictive factors for estimating OS along with PFS in individuals with STAD. We employed the concordance index (C-index) to explore the discrimination efficiency of these two nomograms.

Cells and culture conditions

The AGS and MKN7 cell lines were acquired from cell bank of the Chinese Academy of Sciences and inoculated in RPMI-1640 medium (PM 150110, Procell Life Science &Technology Co,.Ltd) enriched with 10% FBS (Gibco, NY, USA) at 37°C and 5% CO_2 conditions.

Reagents and antibodies

Antibodies against β-actin (#4970, Cell Signaling Technology, USA), Anti-GPX4 (ab18196) bought from Abcam (Cambridge, United States), and secondary antibodies (abs20002) acquired from Absin (Shanghai, China) were used for western blotting experiment.

Transfection

We transfected the cells with small interfering RNAs (siRNAs) against LASTR (siLASTR; LncRNA-Pharma, Shanghai, China) and a negative control (siNC) with the Lipofectamine 2000 system (Invitrogen, United States) as described by the manufacturer. Cells were propagated with LASTR siRNAs for 48 h and harvested for subsequent experiments.

RNA isolation and RT-qPCR

The TRIZOL reagent was employed to purify total RNA from cells (TaKaRa, Beijing, China). After that, cDNA was generated from the RNA via reverse transcription with the Prime Script RT Master Mix reagent (TaKaRa, China), per the instructions of the manufacturer. Afterwards, RT-qPCR was run on the ABI 7500HT Fast Real-Time PCR Platform (Applied Biosystems, CA, USA). The $2^{-\Delta\Delta Ct}$ approach was adopted to determine relative lncRNA expression with GAPDH serving as the normalization control. The oligonucleotide primers for RT-qPCR included: LASTR forward, 5'- GAGAAGACAGTGGGTGAAGTCC-3' and reverse, 5'-GACTCTAGGCACCAGCTGAC-3' and GAPDH forward, 5'-GGAAGCTTGTCATCAATGGAAATC-3', and reverse, 5'-TGATG ACCCTTTTGGCTCCC-3'.

Western blotting assay

We inoculated the GC cells onto 6-cm plates for 48 hours and the harvested them via scrapping. Thereafter, lysis RIPA lysis buffer enriched with protease along with phosphatase inhibitors (Solarbio, Beijing, China was employed lyse the cells for 30 minutes. Thereafter, the cells were span at 12,000 g for 20 minutes at 4°C, and the protein quantitated with the BCA protein assay kit (Beyotime, China). Afterwards, 20μg of the proteins were fractionated on an SDS-PAGE gel and transfer-embedded onto PVDF membranes. Blocking of the membranes was done for two hours using 5% skimmed milk dispersed in TBST. Afterwards, the membranes were inoculated overnight with the indicated primary antibody (1:1000). Next, the membranes were rinsed in TBST for ten minutes, and then inoculated at room temperature with the secondary HRP-conjugated antibodies (1:8000) for two hours. Thereafter, the membranes were rinsed with TBST and the bound antibodies visualized with a chemiluminescence kit (Life Technologies, China) on a Bio-Rad gel imager infrared imaging Platform (ChemiDoc XRS+).

5-ethynyl-2′-deoxyuridine (EdU) incorporation assay

1×10^5 GC cells/well were planted onto 24-well plates, allowed to grow for 48 hours, and inoculated with medium enriched with 50μM EdU (Beyotime, Shanghai, China) for two hours. Thereafter, we fixed the cells (in 4% PFA; Beyotime, Shanghai, China) followed by permeabilization, and then introduced a click reaction mixture (200μL/well) for 30 minutes. Nuclei staining (in Hoechst 33342; 200μL/well) was done for 30 minutes, and a fluorescence microscope employed to visualize the cells.

Colony formation assay

We infected cells with siRNA for two days, and the inoculated 300 cells/well into 6-well dishes and allowed to grow for 10 days. Next, the cells were fixed for 30–60 minutes (in 4% PFA), followed by

staining for 20 minutes (in crystal violet). After numerous washes in ddH2O, the colonies were photographed and their numbers determined.

Transwell migration assay

Cell migration was evaluated using a BD (Franklin Lakes, United States) transwell compartment without Matrigel. Following transfection, we introduced $2x10^5$ cells in serum-free medium onto the upper compartment of the transwell, then medium enriched with 20% FBS was introduced to the lower compartment and allowed to grow for one day. Thereafter, the cells were fixed for 30 minutes with 4% PFA, followed by staining for 20 minutes (in crystal violet) and the rinsed with PBS. We counted the cells in five fields (top, bottom, center, left, and right) under a microscope.

Wound healing assay

The GC cells were planted into 6-well plates and a sterile pipette tip employed to make a scratch. Next, the cells were rinsed with PBS, and then inoculated in medium enriched with 2% FBS. We acquired images at 0 and 24 h with a phase contrast microscope. The fraction of wound healing was determined follows: [1 - (empty area 24 h/empty area 0 h)] × 100%.

Statistical analysis

All data analyzes were implemented in Bioconductor packages in R software, version 4.1.0 and GraphPad Prism 8.0 Software. Unpaired Student's t-test, the Wilcoxon rank-sum test, ANOVA, and the Kruskal–Wallis test were adopted to compare continuous variables. Pearson analysis was implemented for the correlation analyses. $P < 0.05$ denoted statistical significance.

Results

Patient characteristics

Overall, 375 STAD tumor samples along with 32 non-malignant neighboring tissues were analyzed, and their expression profiles were identified. The clinical features of the patients are given in Table 1. Next, 382 ferroptosis-related lncRNAs were obtained from FerrDb (Fig. 1A). Using Pearson's correlation test, 503 differentially expressed ferroptosis-related lncRNAs were obtained (Fig. 1B). To gain profound understanding of how these ferroptosis-related lncRNAs may drive STAD development, we performed GO along with KEGG enrichment analyses. The BPs were related to the response to oxidative stress and response to metal ions. The CCs were related to the production of oxidoreductase complex and NADPH oxidase complexes. The MFs were related to oxidoreductase activity, iron ion binding and superoxide – generating NAD(P)H oxidase activity (Fig. 1C). KEGG-based analysis exhibited main enrichment in ferroptosis, the HIF-1 signaling pathway, the p53 signaling pathway, the PPAR signaling pathway, and the ErbB signaling pathway (Fig. 1D). The enrichment analyses indicated that ferroptosis-related lncRNAs are

closely related to iron metabolism and could mediate some pivotal signaling pathways in tumorigenesis of STAD.

Table 1
The clinical characteristics of patients in the TCGA-STAD dataset.

Variable	Number of samples
Gender	
Male/Female	241/134
Age at diagnosis	
≤ 65/>65/NA	164/207/4
Grade	
G1/G2/G3 /NA	10/137/219/9
Stage	
I/II/III/IV/NA	53/111/150/38/23
T	
T0/T1/T2/T3/T4/NA	19/80/168100/8
N	
N0/N1/N2/N3/NA	111/97/75/74/18
M	
M0/M1/NA	330/25/20

Prognostic value of ferroptosis-related lncRNAs in STAD

The lack of reliable markers for early tumor diagnosis is still one of the key factors in the dismal prognosis of individuals with advanced STAD. Recent findings have revealed that ferroptosis-related lncRNAs can act as prognostic targets in diverse cancers (13, 14). Thus, we further confirmed the possible predictive value of ferroptosis-related lncRNAs in individuals with STAD. Univariate Cox regression uncovered 27 and 40 ferroptosis-related lncRNAs that were remarkably related to OS and PFS, respectively (Fig. 2A,3A). After that, multivariate Cox analysis was carried out, and a total of 25 ferroptosis-related lncRNAs were employed to produce two predictive signatures, consisting of 12 ferroptosis-related lncRNAs for the OS signature, 13 ferroptosis-related lncRNAs for the PFS signature. The time-based ROC curves illustrated that the AUCs of the OS signature for estimating 1-, 3-, and 5-year OS were 0.697, 0.712, and 0.734, respectively (Fig. 2B). Subsequently, based on the median risk score, patients were divided into high- and low-risk group. The K-M plots illustrated that the high-risk group had a dismal OS in comparison with the low-risk group (Fig. 2C). Similarly, the AUCs of the signature for

estimating 1-, 3-, and 5-year PFS were 0.752, 0.803, and 0.771, respectively (Fig. 3B). Similar to the OS signature, the individuals with STAD with higher risk scores had worse PFS (Fig. 3C). These data illustrated that the OS, as well as PFS signature were both valuable tools for estimating the prognosis of individuals with STAD. Besides, to more clearly illustrate differences in the prognosis and expression trends of lncRNAs, we constructed heatmaps (Fig. 2D, 3D), survival status plots (Fig. 2E, 3E), and risk score plots (Fig. 2F, 3F). All of the above indicate that the signatures based on DEFRLs can be used to effectively assess the prognosis of STAD patients.

Creation of nomograms on the basis of the DEFRL signatures and clinical parameters

To enhance the clinical utility of our prognostic signatures, we constructed two comprehensive signatures based on independent clinical parameters. First, we conducted univariate along with multivariate cox analyses to explore independent OS along with PFS predictive variables. We identified risk score, age, as well as stage as independent OS-related variables (Fig. 4A,4B). Three independent variables, including risk score, sex and stage, were identified as PFS-related variables (Fig. 5A,5B). Clinical factors of STAD patients that correlated with DCA parameters were screened (Fig. 4C, 5C). Afterwards, on the basis of the independent predictive variables, two new nomograms were created to estimate OS, as well as PFS (Fig. 4D, 5D). The C-indices were 0.674 (95% CI 0.625–0.723) and 0.664 (95% CI 0.6052–0.7228) for the OS and PFS nomograms, respectively. These data illustrated that two nomograms can be adopted to precisely estimate the prognosis of individuals with STAD. The heatmaps for the relationship of ferroptosis-related lncRNA prognostic signatures with clinicopathological manifestations were also produced (Fig. 4E, 5E). Moreover, the relationship between lncRNAs and mRNAs for the OS and PFS signatures is shown in Fig. 4F and 5F, which show that there is a complicated regulatory relationship between them.

The roles of LASTR in GC

There was one overlapping ferroptosis-related lncRNA (LASTR) among those identified by multivariate regression of OS and PFS signatures, which shows that LASTR is the most critical factor in the STAD prognostic prediction models. It was reported that LASTR could foster fitness of cancer cells via modulating the activity of the U4/U6 recycling factor SART3 (15). We next explored the specific roles of LASTR in GC cells. The expression of LASTR in gastric cancer tissues, along with neighboring non-malignant tissues from the TCGA data resource is given in Fig. 6A. K-M survival curves illustrated that low level of LASTR were associated with remarkably better OS and PFS (Fig. 6B,6C). Two GC cell lines (AGS and MKN7) were chosen to be knocked down using small interfering RNA (siRNA), and the efficiency was confirmed with RT-qPCR (Fig. 7A,7B). Subsequently, EdU incorporation assay (Fig. 7C,7D) and colony formation assay (Fig. 7E,7F) were performed on the two kinds of gastric cancer cells to measure changes in proliferative capacity, wound healing assay (Fig. 8A,8B) and transwell migration assay (Fig. 8C,8D) were carried out to assess changes in migration capacity. The results illustrated that cell proliferation and migration abilities were decreased after LASTR knock down. Western blotting was adopted to explore the expression of the ferroptosis marker GPX4 between knockdown group and control

group (Fig. 8E,8F). The results show that knock down LASTR can repress cell growth, migration and may trigger ferroptosis in GC.

Discussion

Despite advances in detection approaches, as well as medical standards, the five-year survival rate of STAD patients remains very low (16). One of the main reasons is the lack of sufficiently specific and sensitive biomarkers for early diagnosis(17). It has been shown that ferroptosis is involved in STAD proliferation, migration, resistance and other biological behaviors (18–22). LncRNAs are pivotal regulators of ferroptosis, playing different biological roles in different cancer type(7–9, 23–26). However, an effective predictive tool featuring ferroptosis-related lncRNAs for STAD patients is still lacking. Herein, 12 and 13 ferroptosis-related lncRNAs were identified and used to produce signatures to predict OS and PFS, respectively, in STAD patients. First, 382 ferroptosis-related lncRNAs were obtained from the TCGA, 503 lncRNAs were established as candidate predicative biomarkers, and GO and KEGG analyses uncovered the prospective mechanisms of these lncRNAs. Notably, we constructed an OS predictive signature based on 12 key lncRNAs and a PFS predictive signature on the basis of 13 key lncRNAs. As per the respective risk scores, STAD subjects were categorized into high- and low-risk group. The differences in OS and PFS between the high-risk group and low-risk group were both statistically remarkable. The reliability of these two signatures was further supported by the prediction ability of the ROC curves of the two signatures. In addition, we established two comprehensive nomograms integrating the lncRNA-related prognostic signatures and clinical features to enhance clinical utility. These nomograms could allow clinicians to evaluate the OS along with PFS for each STAD patient by inputting the score for each parameter.

In our study, we found that oxidative stress and tumor-linked signaling pathways such as the HIF-1 signaling pathway, the p53 signaling pathway, the PPAR signaling pathway, and the ErbB signaling pathway are significantly enriched through GO and KEGG functional enrichment analysis. It is reported that ferroptosis induced by oxidative stress is associated with various diseases such as Alzheimer's disease(27), intervertebral disc degeneration(28), and cancer(29). Ni et al. found that targeting HIF-1α can induce osteoclast ferroptosis to treat osteoporosis(30). Some studies have shown that p53 can be used to regulate ferroptosis and mediate certain diseases(31, 32). The above studies have proved the regulatory relationship between signaling pathways and ferroptosis in different disease types, which also confirms the trustworthiness of the signatures we have constructed from the side.

Twelve lncRNAs (AC026368.1, CFAP61-AS1, AC090772.1, LINC00449, AC005165.1, LINC01614, AL356215.1, REPIN1-AS1, LASTR, LINC00460, AC015712.1, PVT1) in the OS signature and 13 lncRNAs (AL163953.1, AL356417.2, POLH-AS1, LINC01094, AP002784.1, AL031985.3, LINC01977, LASTR, AC068790.3, AC023024.1, AC124067.4, ZBTB40-IT1, LINC00092) in the PFS signature were identified. LINC00449(33), LINC01614(34–38), LINC00460(39–43), PVT1(23, 25, 44–48), LINC01094(49–54), LINC01977(55), ZBTB40-IT1(56), LINC00092(57) have been reported to regulate the biological behavior or be used as tumor prognostic biomarkers in various cancers. Except for the lncRNAs mentioned above,

there are very few reports on other lncRNAs, which is what we will focus on in the future. Among the OS and PFS signatures, LASTR is the only lncRNA with both signatures, which means that it may have a greater prognostic effect on STAD patients. So next we focused on the biological role of LASTR in GC. Cell experiments, omics experiments, and bio-information analysis were performed to confirm that LASTR has a role in enhancing gastric cancer progression. When verifying the relationship between LASTR and ferroptosis, due to the limitations of experimental technology and experimental environment, we only observed the changes in the ferroptosis marker GPX4 protein after LASTR was knocked down to speculate their regulatory relationships. It is not very rigorous. And we will explore this issue in advanced research settings in the future.

Ferroptosis has increasingly become a hot topic in research in recent years and provides us with a novel mechanism for the treatment of cancer. There are still many unknown areas in the relation between ferroptosis and lncRNAs that are worth exploring. Here, we identified 12 and 13 ferroptosis-related lncRNAs in an OS signature and PFS signature of STAD, respectively, and conducted experimental verification of the roles of LASTR.

Conclusion

In general, novel ferroptosis-related biomarkers were identified for STAD prognosis. One of the markers, LASTR, has been experimentally verified as a cancer-promoting factor and is associated with ferroptosis. This research provides a new perspective for us to treat cancer and predict the survival of cancer patients.

Declarations

Author Contributions

Gongjun Wang and Libin Sun analyzed the data and wrote the manuscript. Shasha Wang, Jing Guo, and Hui Li assisted in editing the manuscript. Ruoxi Xiao, Wenqian Li and Jing Lv contributed to the design of the study. Wensheng Qiu and Weiwei Qi are the corresponding authors of the paper. All authors contributed to the article and approved the submitted version.

Funding

This study was supported by four grants: 1. Beijing Xisike Clinical Oncology Research Foundation (Grant No. Y-BMS2019-038) 2. WU JIEPING Medical Foundation (Grant No.320.6750.19088-29) 3. Shandong Medical and Health Technology Development Foundation (Grant No.202003030451) 4. Qingdao Municipal People's Livelihood Science and Technology Foundation (Grant No.17-3-3-34-nsh)

Acknowledgments

The authors gratefully acknowledge the data provided by patients and researchers participating in TCGA, cBioPortal and FerrDb.

References

1. Bray F, Ferlay J, Soerjomataram I, Siegel R, Torre L, Jemal AJCacjfc. Global cancer statistics 2018: GLOBOCAN estimates of incidence and mortality worldwide for 36 cancers in 185 countries. 2018;68(6):394-424.
2. Chen W, Zheng R, Baade PD, Zhang S, Zeng H, Bray F, et al. Cancer statistics in China, 2015. CA: a cancer journal for clinicians. 2016;66(2):115-32.
3. Van Cutsem E, Sagaert X, Topal B, Haustermans K, Prenen HJL. Gastric cancer. 2016;388(10060):2654-64.
4. Tang D, Kang R, Berghe TV, Vandenabeele P, Kroemer G. The molecular machinery of regulated cell death. Cell research. 2019;29(5):347-64.
5. Stockwell BR, Friedmann Angeli JP, Bayir H, Bush AI, Conrad M, Dixon SJ, et al. Ferroptosis: A Regulated Cell Death Nexus Linking Metabolism, Redox Biology, and Disease. Cell. 2017;171(2):273-85.
6. Hassannia B, Vandenabeele P, Vanden Berghe T. Targeting Ferroptosis to Iron Out Cancer. Cancer cell. 2019;35(6):830-49.
7. Zhang Y, Guo S, Wang S, Li X, Hou D, Li H, et al. LncRNA OIP5-AS1 inhibits ferroptosis in prostate cancer with long-term cadmium exposure through miR-128-3p/SLC7A11 signaling. Ecotoxicology and environmental safety. 2021;220:112376.
8. Ma Q, Dai X, Lu W, Qu X, Liu N, Zhu C. Silencing long non-coding RNA MEG8 inhibits the proliferation and induces the ferroptosis of hemangioma endothelial cells by regulating miR-497-5p/NOTCH2 axis. Biochemical and biophysical research communications. 2021;556:72-8.
9. Wang Z, Chen X, Liu N, Shi Y, Liu Y, Ouyang L, et al. A Nuclear Long Non-Coding RNA LINC00618 Accelerates Ferroptosis in a Manner Dependent upon Apoptosis. Molecular therapy : the journal of the American Society of LncRNA Therapy. 2021;29(1):263-74.
10. Gao J, Aksoy BA, Dogrusoz U, Dresdner G, Gross B, Sumer SO, et al. Integrative analysis of complex cancer genomics and clinical profiles using the cBioPortal. Science signaling. 2013;6(269):pl1.
11. Zhou N, Bao J. FerrDb: a manually curated resource for regulators and markers of ferroptosis and ferroptosis-disease associations. Database : the journal of biological databases and curation. 2020;2020.
12. Yu G, Wang LG, Han Y, He QY. clusterProfiler: an R package for comparing biological themes among lncRNA clusters. Omics : a journal of integrative biology. 2012;16(5):284-7.
13. Cai HJ, Zhuang ZC, Wu Y, Zhang YY, Liu X, Zhuang JF, et al. Development and validation of a ferroptosis-related lncRNAs prognosis signature in colon cancer. Bosnian journal of basic medical sciences. 2021.

14. Tang Y, Li C, Zhang YJ, Wu ZH. Ferroptosis-Related Long Non-Coding RNA signature predicts the prognosis of Head and neck squamous cell carcinoma. International journal of biological sciences. 2021;17(3):702-11.
15. De Troyer L, Zhao P, Pastor T, Baietti MF, Barra J, Vendramin R, et al. Stress-induced lncRNA LASTR fosters cancer cell fitness by regulating the activity of the U4/U6 recycling factor SART3. Nucleic acids research. 2020;48(5):2502-17.
16. Jiang F, Shen X. Current prevalence status of gastric cancer and recent studies on the roles of circular RNAs and methods used to investigate circular RNAs. Cellular & molecular biology letters. 2019;24:53.
17. Dang Y, Ouyang X, Zhang F, Wang K, Lin Y, Sun B, et al. Circular RNAs expression profiles in human gastric cancer. Scientific reports. 2017;7(1):9060.
18. Fu D, Wang C, Yu L, Yu R. Induction of ferroptosis by ATF3 elevation alleviates cisplatin resistance in gastric cancer by restraining Nrf2/Keap1/xCT signaling. Cellular & molecular biology letters. 2021;26(1):26.
19. Gao Z, Deng G, Li Y, Huang H, Sun X, Shi H, et al. Actinidia chinensis Planch prevents proliferation and migration of gastric cancer associated with apoptosis, ferroptosis activation and mesenchymal phenotype suppression. Biomedicine & pharmacotherapy = Biomedecine & pharmacotherapie. 2020;126:110092.
20. Li C, Tian Y, Liang Y, Li Q. Circ_0008035 contributes to cell proliferation and inhibits apoptosis and ferroptosis in gastric cancer via miR-599/EIF4A1 axis. Cancer cell international. 2020;20:84.
21. Zhao D, Zhang C, Jiang M, Wang Y, Liang Y, Wang L, et al. Survival-associated alternative splicing signatures in non-small cell lung cancer. Aging. 2020;12(7):5878-93.
22. Zhang H, Deng T, Liu R, Ning T, Yang H, Liu D, et al. CAF secreted miR-522 suppresses ferroptosis and promotes acquired chemo-resistance in gastric cancer. Molecular cancer. 2020;19(1):43.
23. Lu J, Xu F, Lu H. LncRNA PVT1 regulates ferroptosis through miR-214-mediated TFR1 and p53. Life sciences. 2020;260:118305.
24. Qi W, Li Z, Xia L, Dai J, Zhang Q, Wu C, et al. LncRNA GABPB1-AS1 and GABPB1 regulate oxidative stress during erastin-induced ferroptosis in HepG2 hepatocellular carcinoma cells. Scientific reports. 2019;9(1):16185.
25. Wang M, Mao C, Ouyang L, Liu Y, Lai W, Liu N, et al. Long noncoding RNA LINC00336 inhibits ferroptosis in lung cancer by functioning as a competing endogenous RNA. Cell death and differentiation. 2019;26(11):2329-43.
26. Yang Y, Tai W, Lu N, Li T, Liu Y, Wu W, et al. lncRNA ZFAS1 promotes lung fibroblast-to-myofibroblast transition and ferroptosis via functioning as a ceRNA through miR-150-5p/SLC38A1 axis. 2020;12(10):9085-102.
27. Park MW, Cha HW, Kim J, Kim JH, Yang H, Yoon S, et al. NOX4 promotes ferroptosis of astrocytes by oxidative stress-induced lipid peroxidation via the impairment of mitochondrial metabolism in Alzheimer's diseases. Redox biology. 2021;41:101947.

28. Yang RZ, Xu WN, Zheng HL, Zheng XF, Li B, Jiang LS, et al. Involvement of oxidative stress-induced annulus fibrosus cell and nucleus pulposus cell ferroptosis in intervertebral disc delncRNAration patholncRNAsis. Journal of cellular physiology. 2021;236(4):2725-39.
29. Kou L, Sun R, Jiang X, Lin X, Huang H, Bao S, et al. Tumor Microenvironment-Responsive, Multistaged Liposome Induces Apoptosis and Ferroptosis by Amplifying Oxidative Stress for Enhanced Cancer Therapy. ACS applied materials & interfaces. 2020;12(27):30031-43.
30. Ni S, Yuan Y, Qian Z, Zhong Z, Lv T, Kuang Y, et al. Hypoxia inhibits RANKL-induced ferritinophagy and protects osteoclasts from ferroptosis. Free radical biology & medicine. 2021;169:271-82.
31. Tang LJ, Zhou YJ, Xiong XM, Li NS, Zhang JJ, Luo XJ, et al. Ubiquitin-specific protease 7 promotes ferroptosis via activation of the p53/TfR1 pathway in the rat hearts after ischemia/reperfusion. Free radical biology & medicine. 2021;162:339-52.
32. Zhang Z, Guo M, Shen M, Kong D, Zhang F, Shao J, et al. The BRD7-P53-SLC25A28 axis regulates ferroptosis in hepatic stellate cells. Redox biology. 2020;36:101619.
33. Shi Y, Zhu Y, Zheng X, Zheng Z. LINC00449 regulates the proliferation and invasion of acute monocytic leukemia and predicts favorable prognosis. Journal of cellular physiology. 2020;235(10):6536-47.
34. Cai Q, Zhao X, Wang Y, Li S, Wang J, Xin Z, et al. LINC01614 promotes osteosarcoma progression via miR-520a-3p/SNX3 axis. Cellular signalling. 2021;83:109985.
35. Chen Y, Cheng WY, Shi H, Huang S, Chen H, Liu D, et al. Classifying gastric cancer using FLORA reveals clinically relevant molecular subtypes and highlights LINC01614 as a biomarker for patient prognosis. OncolncRNA. 2021;40(16):2898-909.
36. Liu AN, Qu HJ, Yu CY, Sun P. Knockdown of LINC01614 inhibits lung adenocarcinoma cell progression by up-regulating miR-217 and down-regulating FOXP1. Journal of cellular and molecular medicine. 2018;22(9):4034-44.
37. Tang L, Chen Y, Peng X, Zhou Y, Jiang H, Wang G, et al. Identification and Validation of Potential Pathogenic LncRNAs and Prognostic Markers in ESCC by Integrated Bioinformatics Analysis. Frontiers in lncRNAtics. 2020;11:521004.
38. Wang Y, Song B, Zhu L, Zhang X. Long non-coding RNA, LINC01614 as a potential biomarker for prognostic prediction in breast cancer. PeerJ. 2019;7:e7976.
39. Cheng J, Lou Y, Jiang K. Downregulation of long non-coding RNA LINC00460 inhibits the proliferation, migration and invasion, and promotes apoptosis of pancreatic cancer cells via modulation of the miR-320b/ARF1 axis. Bioengineered. 2021;12(1):96-107.
40. Hong H, Sui C, Qian T, Xu X, Zhu X, Fei Q, et al. Long noncoding RNA LINC00460 conduces to tumor growth and metastasis of hepatocellular carcinoma through miR-342-3p-dependent AGR2 up-regulation. Aging. 2020;12(11):10544-55.
41. Hou P, Meng S, Li M, Lin T, Chu S, Li Z, et al. LINC00460/DHX9/IGF2BP2 complex promotes colorectal cancer proliferation and metastasis by mediating HMGA1 mRNA stability depending on m6A modification. Journal of experimental & clinical cancer research : CR. 2021;40(1):52.

42. Jiang Y, Cao W, Wu K, Qin X, Wang X, Li Y, et al. LncRNA LINC00460 promotes EMT in head and neck squamous cell carcinoma by facilitating peroxiredoxin-1 into the nucleus. Journal of experimental & clinical cancer research : CR. 2019;38(1):365.
43. Li F, Zhu W, Wang Z. Long noncoding RNA LINC00460 promotes the progression of cervical cancer via regulation of the miR-361-3p/Gli1 axis. Human cell. 2021;34(1):229-37.
44. Cho SW, Xu J, Sun R, Mumbach MR, Carter AC, Chen YG, et al. Promoter of lncRNA LncRNA PVT1 Is a Tumor-Suppressor DNA Boundary Element. Cell. 2018;173(6):1398-412.e22.
45. Ghetti M, Vannini I, Storlazzi CT, Martinelli G, Simonetti G. Linear and circular PVT1 in hematological malignancies and immune response: two faces of the same coin. Molecular cancer. 2020;19(1):69.
46. Shigeyasu K, Toden S, Ozawa T, Matsuyama T, Nagasaka T, Ishikawa T, et al. The PVT1 lncRNA is a novel epilncRNAtic enhancer of MYC, and a promising risk-stratification biomarker in colorectal cancer. Molecular cancer. 2020;19(1):155.
47. Xu Y, Li Y, Jin J, Han G, Sun C, Pizzi MP, et al. LncRNA PVT1 up-regulation is a poor prognosticator and serves as a therapeutic target in esophageal adenocarcinoma. Molecular cancer. 2019;18(1):141.
48. Zhou C, Yi C, Yi Y, Qin W, Yan Y, Dong X, et al. LncRNA PVT1 promotes gemcitabine resistance of pancreatic cancer via activating Wnt/β-catenin and autophagy pathway through modulating the miR-619-5p/Pygo2 and miR-619-5p/ATG14 axes. Molecular cancer. 2020;19(1):118.
49. Jiang Y, Li W, Yan Y, Yao X, Gu W, Zhang H. LINC01094 triggers radio-resistance in clear cell renal cell carcinoma via miR-577/CHEK2/FOXM1 axis. Cancer cell international. 2020;20:274.
50. Jiang Y, Zhang H, Li W, Yan Y, Yao X, Gu W. FOXM1-Activated LINC01094 Promotes Clear Cell Renal Cell Carcinoma Development via MicroRNA 224-5p/CHSY1. Molecular and cellular biology. 2020;40(3).
51. Li XX, Yu Q. Linc01094 Accelerates the Growth and Metastatic-Related Traits of Glioblastoma by Sponging miR-126-5p. OncoTargets and therapy. 2020;13:9917-28.
52. Xu H, Wang X, Wu J, Ji H, Chen Z, Guo H, et al. Long Non-coding RNA LINC01094 Promotes the Development of Clear Cell Renal Cell Carcinoma by Upregulating SLC2A3 via MicroRNA-184. Frontiers in lncRNAtics. 2020;11:562967.
53. Xu J, Zhang P, Sun H, Liu Y. LINC01094/miR-577 axis regulates the progression of ovarian cancer. Journal of ovarian research. 2020;13(1):122.
54. Zhu B, Liu W, Liu H, Xu Q, Xu W. LINC01094 Down-Regulates miR-330-3p and Enhances the Expression of MSI1 to Promote the Progression of Glioma. Cancer management and research. 2020;12:6511-21.
55. Li Z, Li Y, Wang X, Liang Y, Luo D, Han D, et al. LINC01977 Promotes Breast Cancer Progression and Chemoresistance to Doxorubicin by Targeting miR-212-3p/GOLM1 Axis. Frontiers in oncology. 2021;11:657094.
56. Mei B, Wang Y, Ye W, Huang H, Zhou Q, Chen Y, et al. LncRNA ZBTB40-IT1 modulated by osteoporosis GWAS risk SNPs suppresses osteolncRNAsis. Human lncRNAtics. 2019;138(2):151-66.

57. Zhao L, Ji G, Le X, Wang C, Xu L, Feng M, et al. Long Noncoding RNA LINC00092 Acts in Cancer-Associated Fibroblasts to Drive Glycolysis and Progression of Ovarian Cancer. Cancer research. 2017;77(6):1369-82.

Figures

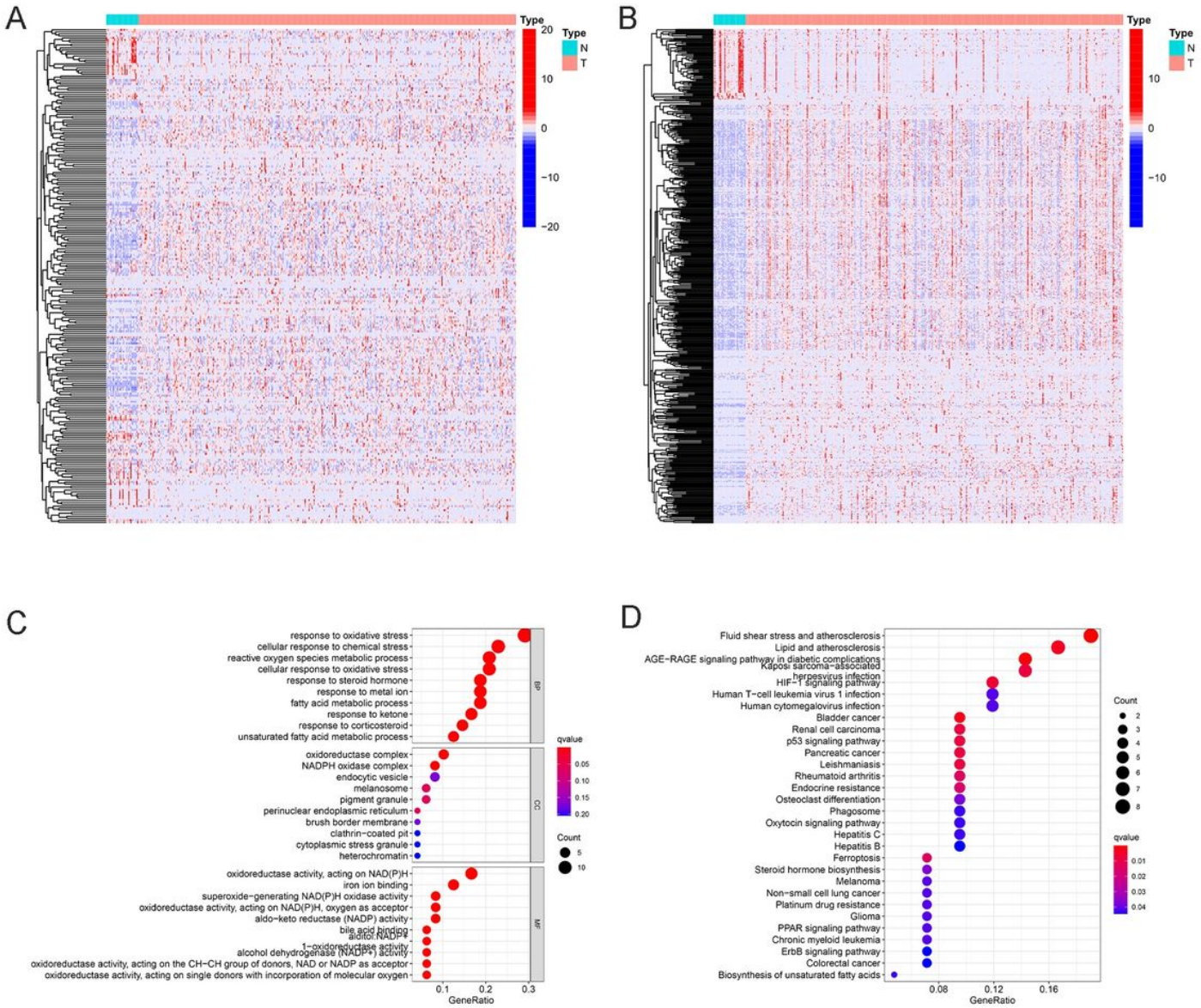

Figure 1

Expression and enrichment analyses of differentially expressed lncRNAs in individuals with stomach adenocarcinoma. (A) Heatmap of ferroptosis-related genes. (B) Heatmap of ferroptosis-related lncRNAs. (C) Bubble chart illustrating the top ten most remarkable terms in the GO, consisting of BP, CC, and MF;

the x-axis refers to the ratio of lncRNAs that are abundant in the matching function. (D) Bubble chart illustrating the top 30 most remarkable terms in KEGG pathway of ferroptosis-related lncRNAs; the x-axis refers to the ratio of lncRNAs that are abundant in the matching function.

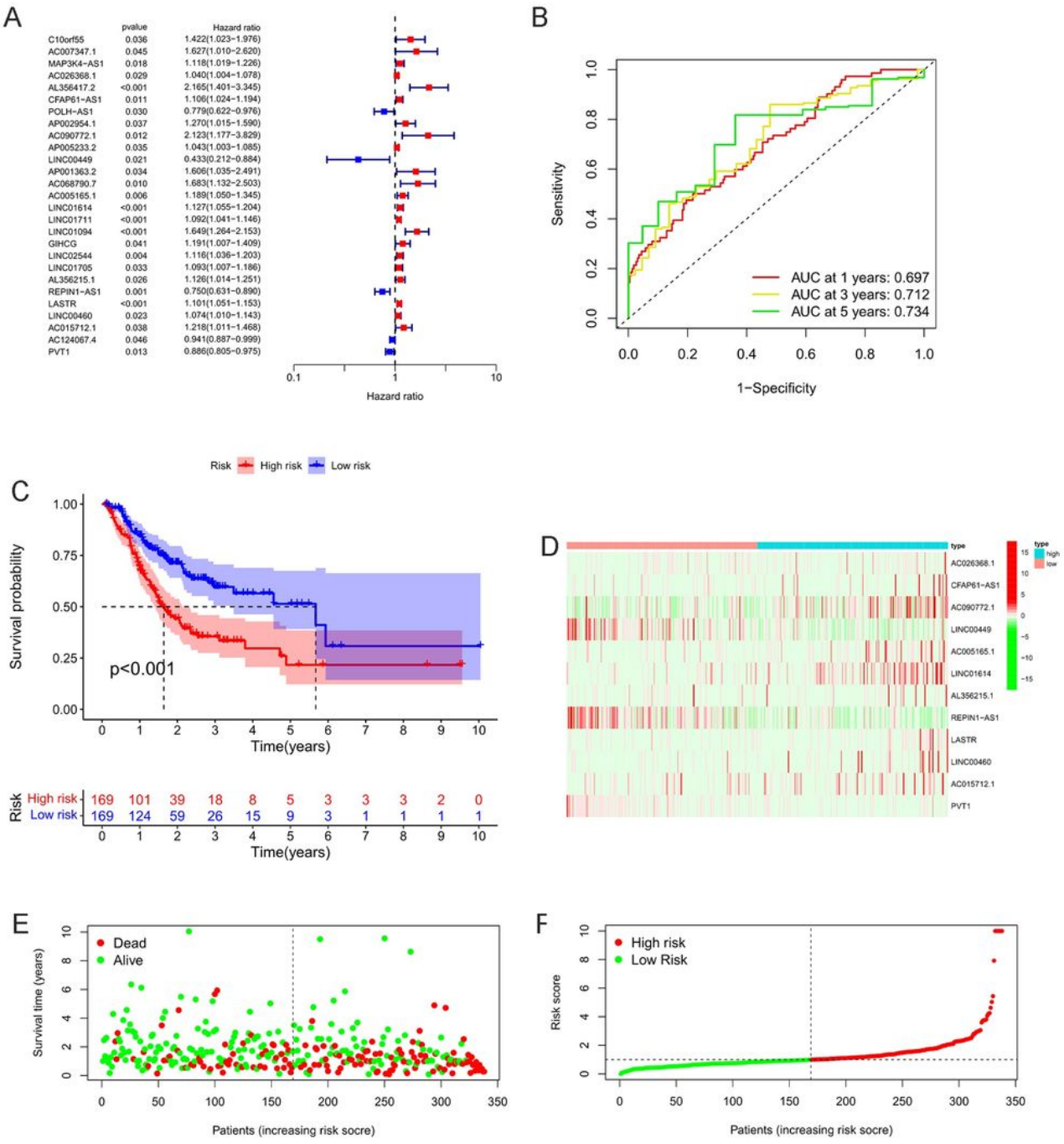

Figure 2

Establishment of 12-DEFRL-based OS signature. (A) Univariate Cox regression analysis established 27 ferroptosis-related lncRNAs that were remarkably associated with OS. (B) Time-based ROC curves of the

OS signature at 1, 3 and 5 years. (C) Kaplan–Meier survival plots illustrating the differences of OS between low-risk and high-risk group. (D) Levels of expression of lncRNAs in high-risk group and low-risk group with the OS signature. (E) OS scatter plots for individuals with stomach adenocarcinoma. (F) Risk score distribution of patients with the OS signature.

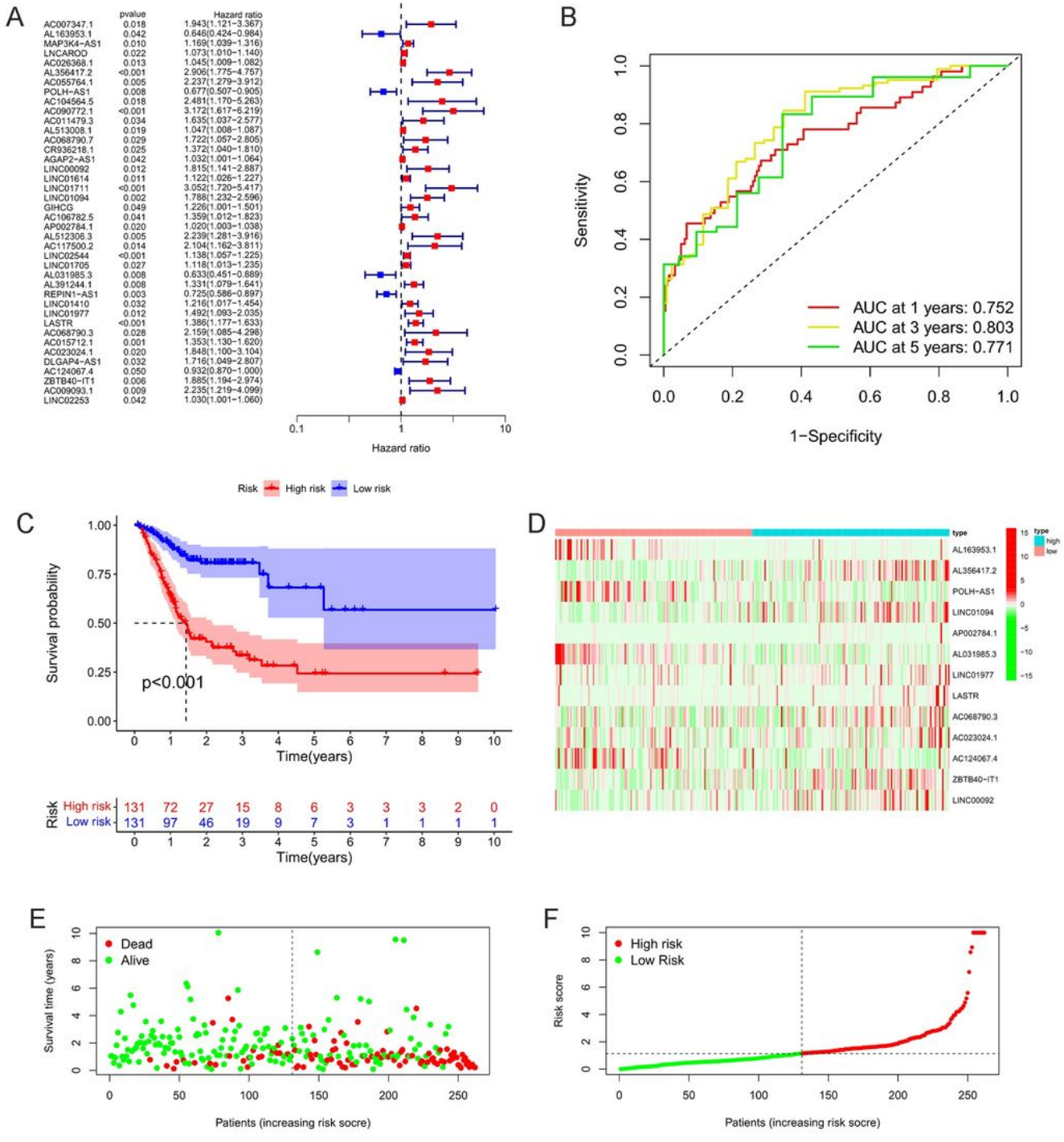

Figure 3

Establishment of 13-DEFRL-based PFS signature. (A) Univariate Cox regression of the uncovered 40 ferroptosis-related lncRNAs that were remarkably associated with PFS. (B) Time-based ROC curves of the PFS signature at 1, 3, and 5 years. (C) Kaplan–Meier survival plots illustrating the differences of PFS between low-risk group and high-risk group. (D) Levels of lncRNAs expression in the high-risk group and low-risk group with the PFS signature. (E) PFS scatter plots for individuals with stomach adenocarcinoma. (F) Risk score distribution of patients with the PFS signature.

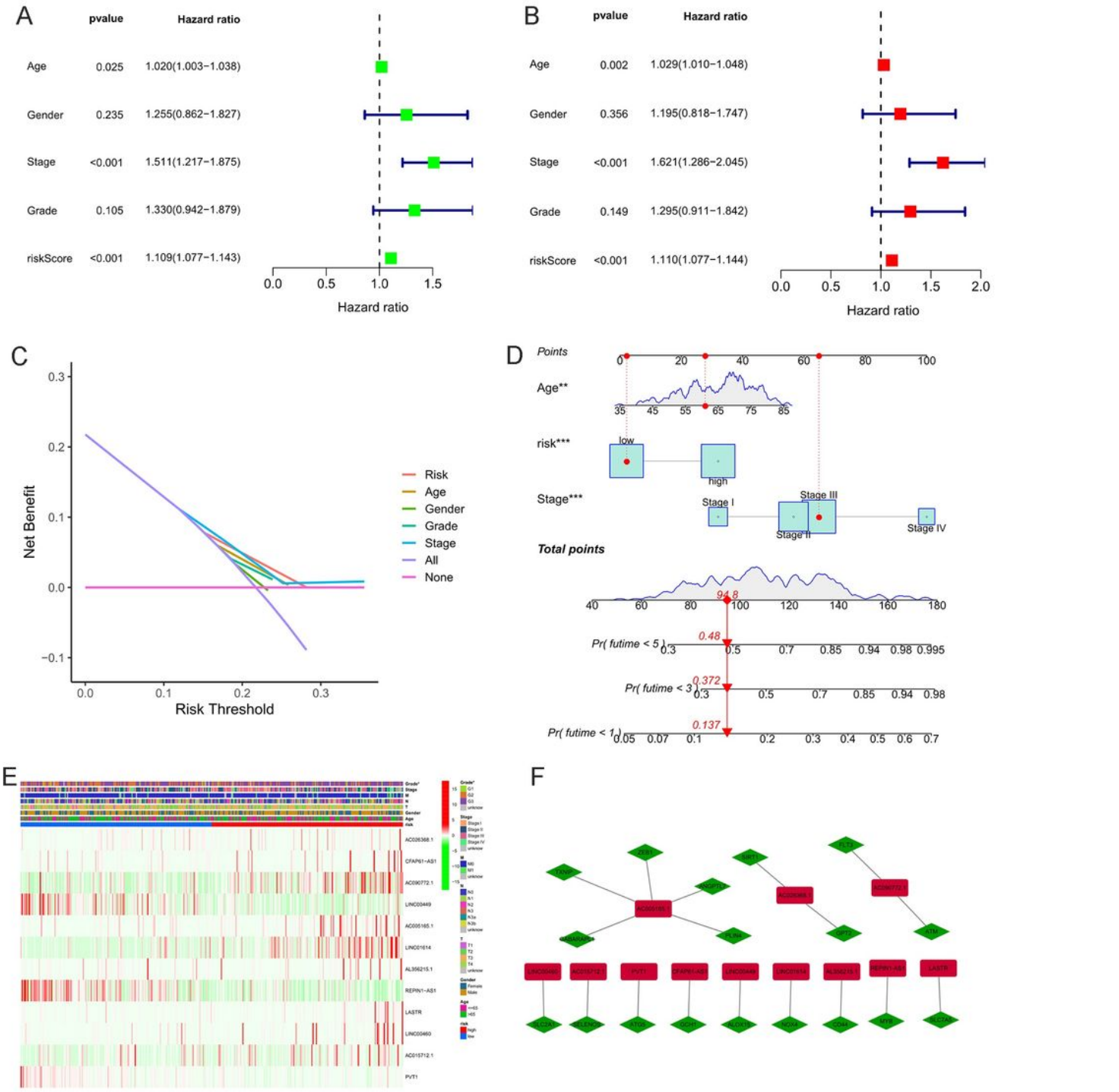

Figure 4

Development of nomogram combining DEFRL-based signature with independent predictive clinical variables to estimate OS in individuals with stomach adenocarcinoma. (A) Univariate regression of DEFRL-based prognostic signature along with clinical factors. (B)Multivariate regression of the remarkable factors in the univariate regression. (C) The DCA of the risk factors with OS. (D) Nomogram of OS integrating OS signature with the two clinical variables of patients (E) Heatmap illustrating ferroptosis-related lncRNAs OS signature and clinicopathological manifestations. (F) The regulatory network of ferroptosis-related genes and OS-linked ferroptosis-related lncRNAs.

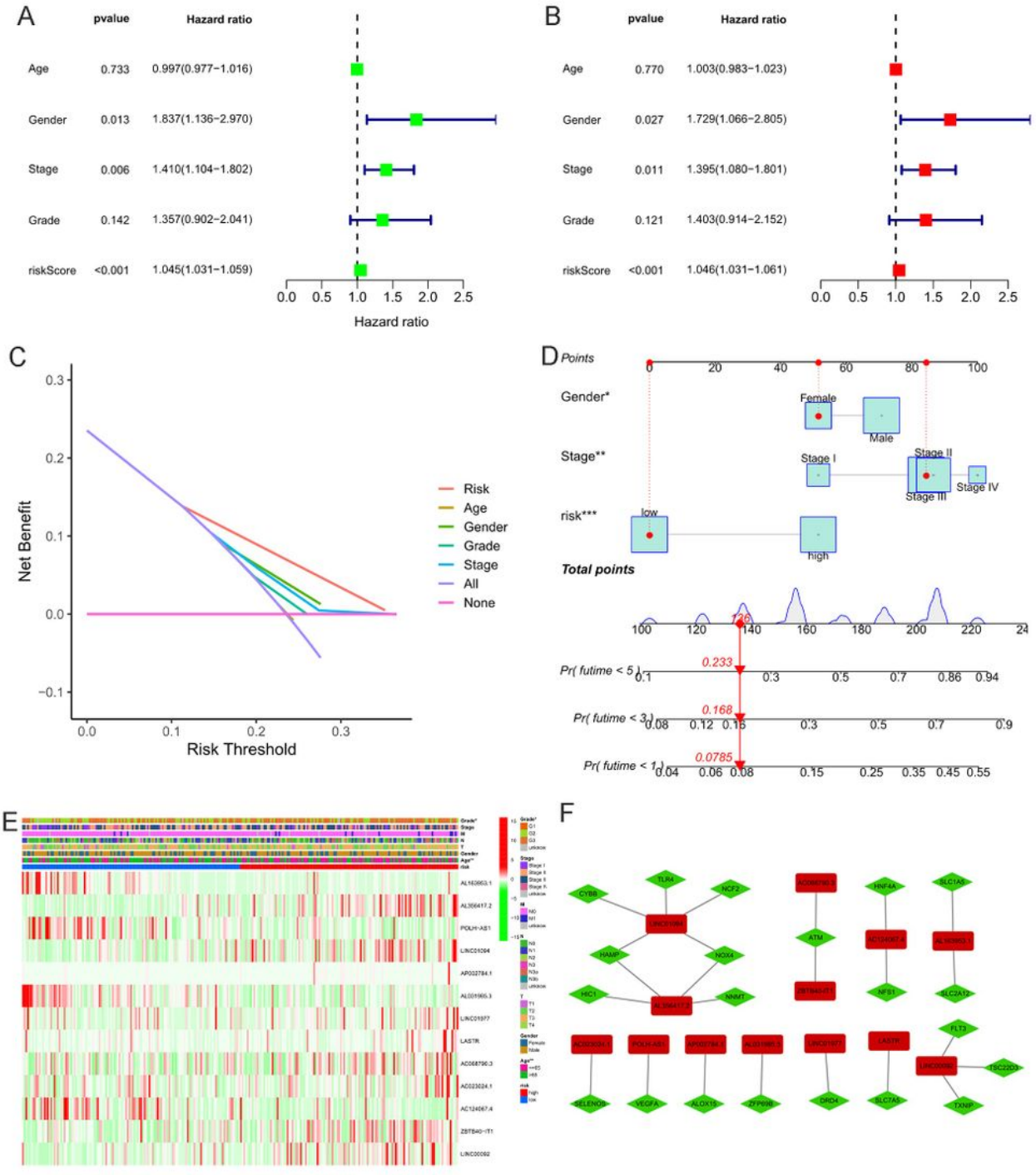

Figure 5

Development of nomogram combining DEFR-based signature with independent predictive clinical variables to predict PFS in individuals with stomach adenocarcinoma. (A) Univariate regression of the DEFRL-based predicative signature along with clinical factors. (B)Multivariate regression of the remarkable factors in the univariate Cox analyses. (C) The DCA of the risk factors with PFS. (D) Nomogram of PFS integrating the PFS signature with the two clinical variables of patients. (E) Heatmap illustrating ferroptosis-related lncRNAs PFS signature and clinicopathological manifestations. (F) The modulatory network of ferroptosis-related genes and PFS-linked ferroptosis-related lncRNAs.

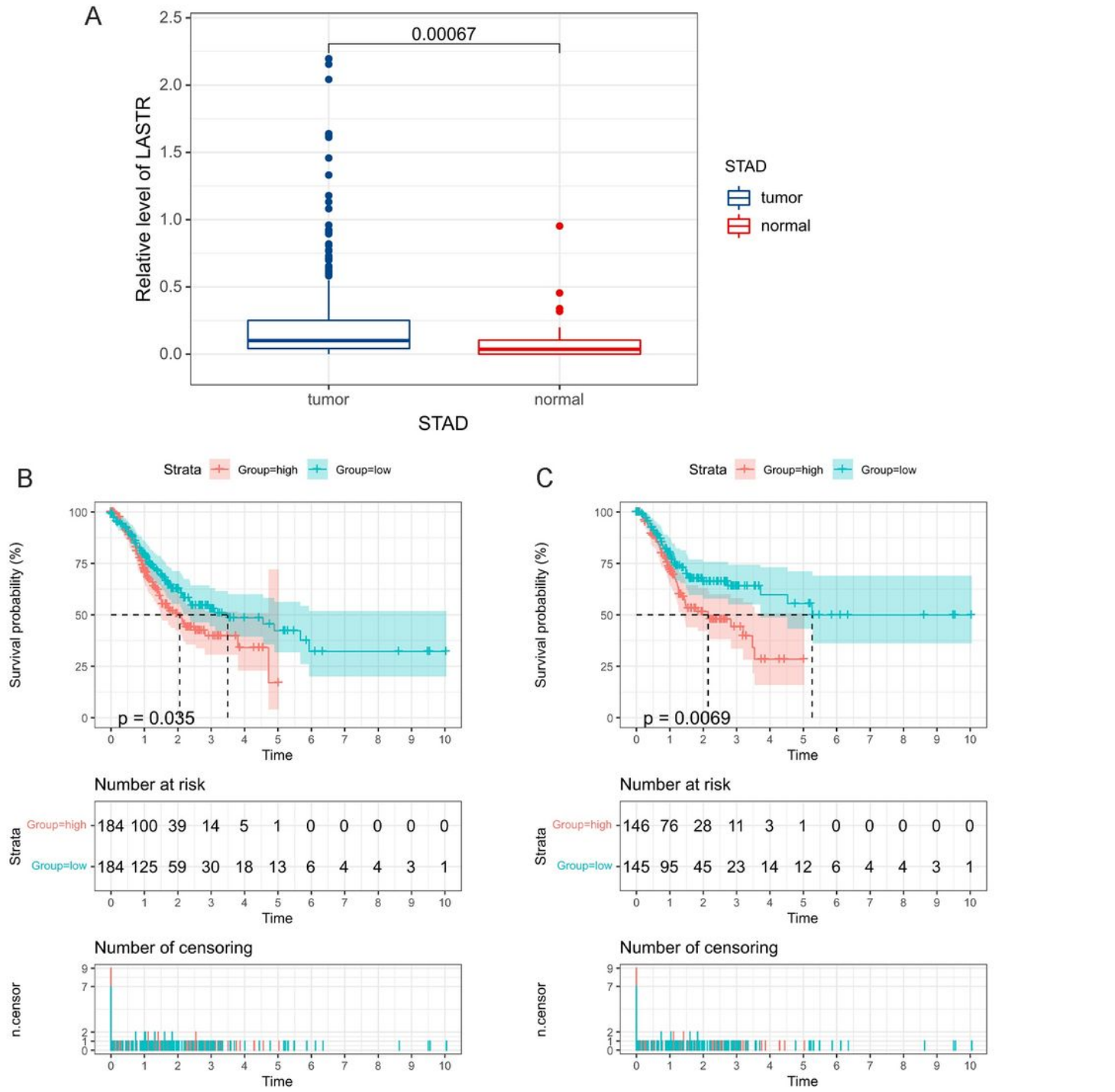

Figure 6

High expression of LASTR predicts poor prognosis in individuals with stomach adenocarcinoma patients. (A) LASTR expression in gastric cancer tissues along with neighboring non-malignant tissues from the TCGA database. (B) Kaplan–Meier survival plots illustrating the differences of OS between low-level and high-level LASTR. (C) Kaplan–Meier survival plots illustrating the differences in PFS between low-level and high-level LASTR.

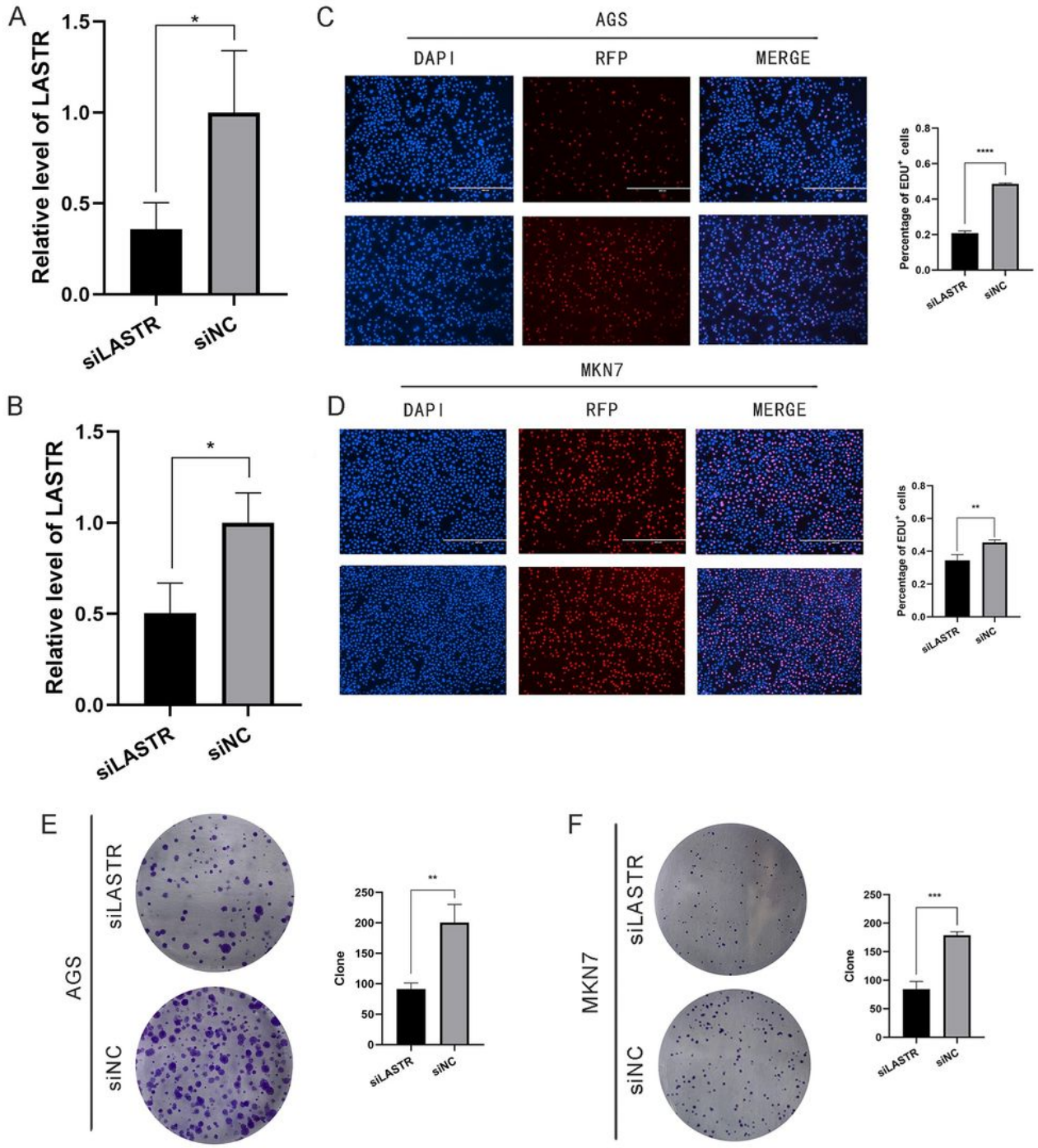

Figure 7

Impact of LASTR knockdown on the growth of GC cells. (A)(B) qPCR analysis of LASTR RNA expression of AGS or MKN7 cells transfected with siLASTR and siNC. (C)(D) Comparison of the proliferative potential between the siLASTR and siNC groups of AGS or MKN7 cells by a EdU incorporation assay. (E)(F) Comparison of the proliferative potential between the siLASTR and siNC groups of AGS or MKN7 cells by a colony formation assay.

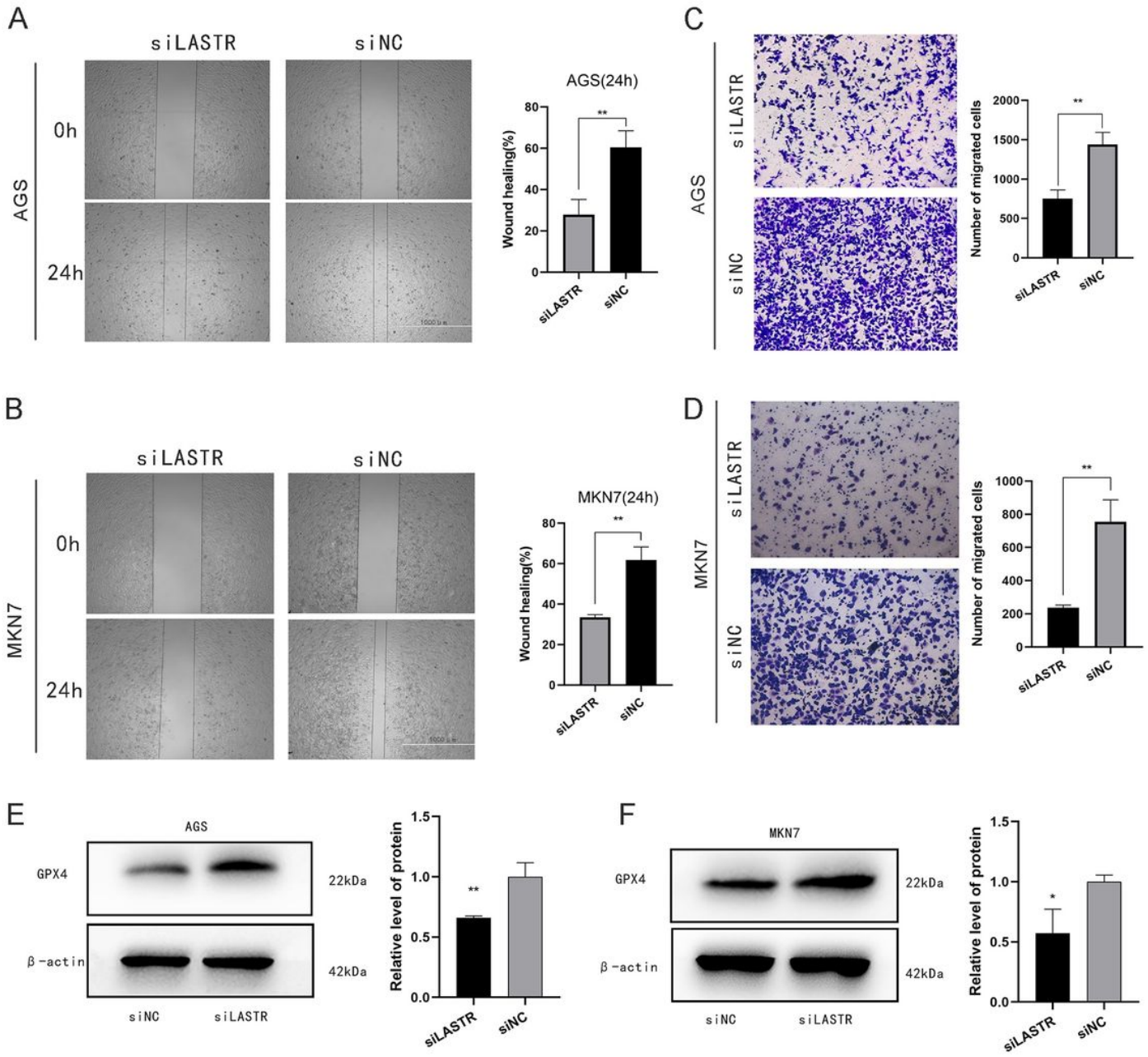

Figure 8

Impact of LASTR knockdown on the migration along with the ferroptosis of GC cells. (A)(B) Wound-healing assay comparing the migration distance between the siLASTR and siNC groups of AGS or MKN7 cells. (C)(D) The transwell assay comparing the number of migration cells between the siLASTR and siNC groups of AGS or MKN7 cells. (E)(F) Comparison of the protein expression of GPX4 between the siLASTR and siNC groups of AGS or MKN7 cells by Western blotting assay.